Skyrmions in thin films with easy-plane magnetocrystalline anisotropy

Mark Vousden,[1] Maximilian Albert,[1] Marijan Beg,[1] Marc-Antonio Bisotti,[1] Rebecca Carey,[1] Dmitri Chernyshenko,[1] David Cortés-Ortuño,[1] Weiwei Wang,[2] Ondrej Hovorka,[1] Christopher H. Marrows,[3] and Hans Fangohr[1]

[1)] *Faculty of Engineering and the Environment, University of Southampton, Southampton, SO16 7QF, United Kingdom.*

[2)] *Department of Physics, Ningbo University, Ningbo 315211, China*

[3)] *School of Physics & Astronomy, University of Leeds, Leeds LS2 9JT, United Kingdom.*

(Dated: 25 April 2016)

We demonstrate that chiral skyrmionic magnetization configurations can be found as the minimum energy state in B20 thin film materials with easy-plane magnetocrystalline anisotropy with an applied magnetic field perpendicular to the film plane. Our observations contradict results from prior analytical work, but are compatible with recent experimental investigations. The size of the observed skyrmions increases with the easy-plane magnetocrystalline anisotropy. We use a full micromagnetic model including demagnetization and a three-dimensional geometry to find local energy minimum (metastable) magnetization configurations using numerical damped time integration. We explore the phase space of the system and start simulations from a variety of initial magnetization configurations to present a systematic overview of anisotropy and magnetic field parameters for which skyrmions are metastable and global energy minimum (stable) states.

arXiv:1602.02064v2 [cond-mat.mtrl-sci] 22 Apr 2016

Skyrmions are topological defects[1] that can be observed in the magnetization configuration of materials that lack inversion symmetry,[2] either due to a non-centrosymmetric crystal lattice,[3,4] or at interfaces between different materials.[5] This lack of inversion symmetry results in a chiral interaction known as the Dzyaloshinskii-Moriya (DM) interaction.[3,4] The DM interaction results in a rich variety of chiral magnetization configurations, including helical, conical, and skyrmionic magnetization configurations. Skyrmionic configurations were predicted[6] and later observed in helimagnetic materials,[7–10] and materials with an interfacial DM interaction.[11–15]

Skyrmions demonstrate potential for applications in data storage and processing devices. Skyrmions have been observed with diameters of the order of atom spacings in mono-atomic Fe layers,[16] which is significantly smaller than the magnetic domains proposed for the racetrack memory design.[17] This results in a greater storage density. The movement of skyrmions has also been demonstrated[18,19] using spin-polarized current densities of the order $10^6\,\mathrm{Am}^{-2}$, which is orders of magnitude less than what is required to move magnetic domain walls.[17,20] These observations demonstrate potential for skyrmion-based racetrack memory technology[21] and other data storage and processing devices.[22]

Certain material restrictions need to be overcome before skyrmions can be used in such technologies. While skyrmions can be stabilized, they are only stable in a limited region of the parameter space defined by an applied magnetic field and the temperature. This region is narrow in bulk materials,[7] larger in thin film materials,[9] and further stabilized in laterally confined geometries[23] and materials with pinning defects.[24] Analytical analysis of helimagnetic thin film material models find that skyrmion lattice states are ground states in helimagnetic thin films with an applied magnetic field only in systems with easy-axis magnetocrystalline anisotropy,[2,25] where the easy axis and the applied field are perpendicular to the plane of the film. However, simulated annealing methods find that skyrmions can be the ground state in two-dimensional helimagnetic thin films with easy-plane anisotropy.[26] Skyrmions have also been identified in two-dimensional surface-inversion breaking systems with easy-plane anisotropy and Rashba spin-orbit coupling.[27] Furthermore, experimental studies of easy-plane helimagnetic thin films identify an additional contribution to the Hall resistivity beyond the ordinary and anomalous contributions.[28–33] This may be interpreted as the topological Hall effect, which arises through real space Berry phase effects,[34,35] and is an indication of potential skyrmion presence. Skyrmions have been directly observed with Lorentz transmission electron microscopy (LTEM) in easy-plane MnSi with the field applied along all principal crystallographic directions.[36]

In this letter, prior analyses are extended by considering a three-dimensional thin film with demagnetization to determine whether or not skyrmions are stable in thin films with easy-plane anisotropy. For a magnetization configuration to be stable, it must be a configuration with the lowest possible energy. Variational techniques have been used to minimize the energy in simplified model systems analytically.[37] Here we use numerical simulation methods to solve a more complete model system.

We consider a cuboidal simulation cell representing a thin film of $Fe_{0.7}Co_{0.3}Si$. The cell has lateral dimensions L_x and L_y, and finite thickness $L_z \ll L_x, L_y$, where x, y, and z are Cartesian axes with origin at the center of the geometry. L_x is equal to the helical period, and $L_y = L_x\sqrt{3}$ to support hexagonal skyrmion lattice magnetization configurations in the simulation cell. Periodic boundary conditions are imposed on the Heisenberg and DM exchange interactions in the lateral directions. The macrogeometry approach[38] is used to model periodicity of the demagnetizing field, with a disc macrogeometry of radius equal to 26 times the helical period and thick-

ness $L_z = 5\,\mathrm{nm}$. The boundary conditions pose a mathematically different problem from analytical work conducted previously, which considers rotationally symmetric magnetization.[2] Our method allows arbitrary magnetization configurations that do not satisfy this symmetry, such as helical states.

The standard numerical micromagnetics approach of solving the Landau-Lifshitz-Gilbert (LLG) equation as an initial value problem is employed here. Unlike previous work, demagnetization effects are incorporated in this energy model since demagnetization is known to affect the stability of skyrmions.[23] A three-dimensional simulation domain with finite thickness is used because magnetization variation in the thickness direction can stabilize skyrmionic configurations.[39] These extensions differentiate this study from previous works.[2,25,26]

The micromagnetic representation of the system energy is modelled here as

$$W(\mathbf{m}) = \int_V \left(w_\mathrm{e} + w_\mathrm{dmi} + w_\mathrm{z} + w_\mathrm{a} + w_\mathrm{d}\right)\,\mathrm{d}V, \qquad (1)$$

where V is a cuboid region of volume $L_x \times L_y \times L_z$, and $\mathbf{m}(x,y,z) = \mathbf{M}(x,y,z)/M_\mathrm{S}$ is the magnetization vector field normalized by saturation magnetization M_S such that $|\mathbf{m}| = 1$. The terms $w_\mathrm{e} = A\,(\nabla\mathbf{m})^2$ and $w_\mathrm{dmi} = D\mathbf{m}\cdot(\nabla\times\mathbf{m})$ are the energy density contributions from Heisenberg and DM exchange interactions respectively. The term $w_\mathrm{z} = -\mu_0 M_\mathrm{S}\mathbf{H}\cdot\mathbf{m}$ is the Zeeman energy density contribution from the applied magnetic field. The term $w_\mathrm{a} = K_1(1-(\mathbf{m}\cdot\hat{\mathbf{z}})^2)$ is the energy density contribution from the magnetocrystalline anisotropy. This anisotropy is easy-axis when $K_1 > 0$ and is easy-plane when $K_1 < 0$. The term $w_\mathrm{d} = -\mu_0 M_\mathrm{S}(\mathbf{H}_\mathrm{d}\cdot\mathbf{m})/2$ is the energy density contribution from demagnetization, where the demagnetizing field $\mathbf{H}_\mathrm{d}$ is calculated using the Fredkin-Koehler finite element method-boundary element method (FEMBEM).[40]

The energy model uses material parameters from experiments on $Fe_{0.7}Co_{0.3}Si$[30,41] as follows: the symmetric exchange coefficient $A = 4.0\times10^{-13}\,\mathrm{Jm^{-1}}$, the DM exchange coefficient $D = 2.7\times10^{-4}\,\mathrm{Jm^{-2}}$, the magnetocrystalline anisotropy coefficient $K_1 = -3.0\times10^{4}\,\mathrm{Jm^{-3}}$, and the saturation magnetization $M_\mathrm{S} = 9.5\times10^{4}\,\mathrm{Am^{-1}}$. To obtain a systematic data set and understanding, the magnetocrystalline anisotropy K_1 is varied in the range $[-0.5K_0, 1.25K_0]$, where $K_0 = D^2/A = 1.8\times10^{5}\,\mathrm{Jm^{-3}}$. This range contains the anisotropy value $K_1 = -0.16K_0$ calculated for $Fe_{0.7}Co_{0.3}Si$. The applied field parallel to the z direction $|\mathbf{H}|$, is varied in the range $[0, 15.4M_\mathrm{S}]$.

Multiple initial magnetization configurations are used to determine the minimum energy state of the micromagnetic system for each combination of $|\mathbf{H}|$ and K_1 values. These initial states are shown in Fig. 1. A finite element method-based simulator has been used to solve the damped LLG equation as an initial value problem for the aforementioned system. The simulator is similar to the software Nmag[42] and uses the FEniCS[43] finite element framework. The edge lengths of the tetrahedral elements of the finite element mesh do not exceed one nanometer, which is chosen to be smaller than both the Bloch parameter $\sqrt{A/|K_1|} > 1.3\,\mathrm{nm}$ and the exchange length $\sqrt{2A/\mu_0 M_\mathrm{S}^2} = 8.4\,\mathrm{nm}$ to correctly resolve micromagnetic behavior. The same finite element mesh is used to discretize the magnetization domain for all results reported here. When the magnetization precesses more slowly than $1\,^\circ\mathrm{ns^{-1}}$ everywhere, it is considered relaxed. All initial configurations shown in Fig. 1 are relaxed independently for each pair of $|\mathbf{H}|$ and K_1 values. The energies of all relaxed configurations at the same $|\mathbf{H}|$ and K_1 are compared, and the configuration with the lowest energy out of all these states is classified as the ground state. A selection of these states are shown in Fig. 2 (a) to (f). Table I shows the normalized $|\mathbf{H}|$ and K_1 values for each of the six configurations (a) to (f).

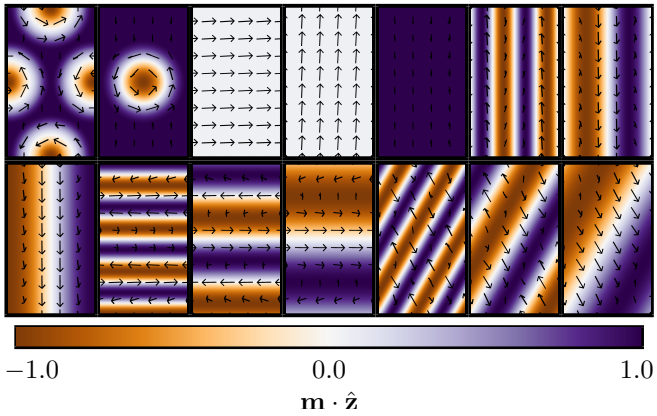

FIG. 1. Initial magnetization configurations to be relaxed using damped Landau-Lifshitz-Gilbert (LLG) dynamics. From the top, left to right, these are hexagonal and rectangular skyrmion lattice states, canted uniform states parallel to the x, y, and z directions, and a variety of helical states. The period of the helices is varied to support metastable states with different helical periods.

Fig. 2 (top) shows a phase diagram which groups relaxed configurations into uniform, skyrmionic, helical, and unclassified configurations. This phase diagram shows the obtained ground state configuration for each point in the applied field and anisotropy parameter space. The locations of the ground states shown in Fig. 2 (a) to (f) are indicated in the phase diagram.

States are considered as uniform if $\mathbf{m}\cdot\bar{\mathbf{m}} > 0.85$ everywhere, where $\bar{\mathbf{m}}$ is the spatially-averaged magnetization direction. States are considered skyrmionic if the skyrmion number $S(\mathbf{m}) > 0.5$, where

$$S(\mathbf{m}) = \frac{1}{4\pi}\int_T \mathbf{m}\cdot\left(\frac{\partial\mathbf{m}}{\partial x}\times\frac{\partial\mathbf{m}}{\partial y}\right)\mathrm{d}x\,\mathrm{d}y, \qquad (2)$$

and T is the surface at $z = 0$ contained by V. States are considered helical if the magnetization configuration contains a full rotation along a single direction in the thin film. Magnetization configurations that do not sat-

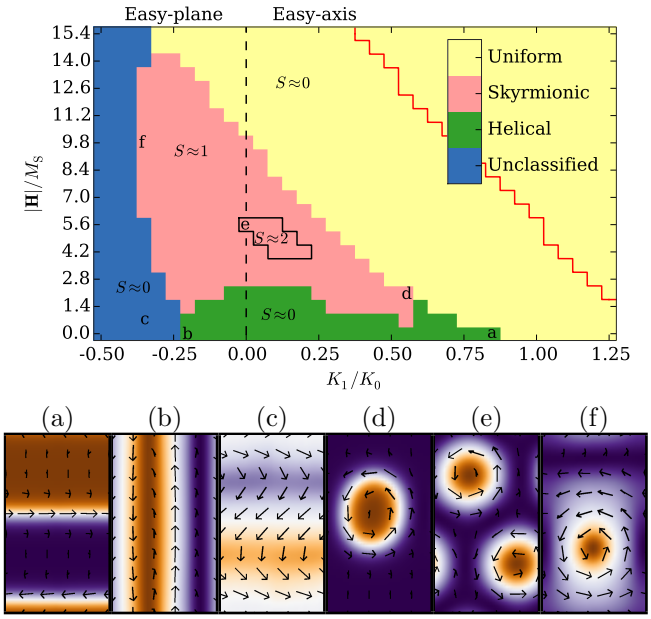

FIG. 2. Top: Phase diagram showing ground state variation with normalized anisotropy K_1/K_0 and applied field magnitude $|\mathbf{H}|/M_S$. Skyrmions are ground states in both easy-plane and easy-axis anisotropy regions. Parameters below the solid line in the uniform region support metastable skyrmionic states. Bottom: Selected magnetization configurations.

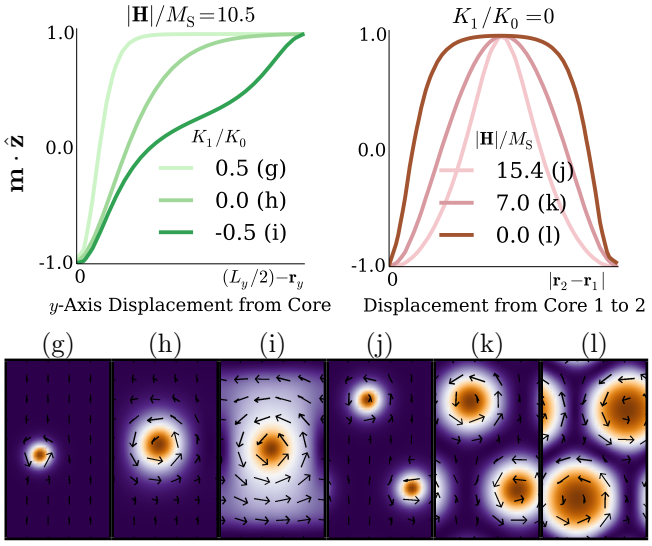

FIG. 3. Top: Metastable skyrmion profiles varying with anisotropy in the rectangular lattice (left), and applied field magnitude in the hexagonal lattice (right), where $\mathbf{r}$ is the coordinate of the skyrmion core. Bottom: Magnetization configurations of the profiles shown above.

isfy any of these conditions are unclassified, but are still considered when energies of relaxed states are compared.

The helical configuration is found for anisotropy values K_1 in the range $[-0.2K_0, 0.85K_0]$, and weak applied fields, in agreement with previous predictions[44] and observations.[9] The uniform state is observed when the applied field and easy-axis anisotropy dominate, and these states have magnetization aligned with the out-of-plane direction (z). This is expected, since the energy contributions from the applied field and the easy-axis magnetocrystalline anisotropy are minimized in this case. The magnetization configurations in the unclassified region, exemplified by Fig. 2 (c), are driven by the easy-plane anisotropy contribution, which causes the magnetization to orient mostly within the plane of the thin-film.

Skyrmion lattice states (Fig. 2 (d) to (f)) are minimum energy states for both positive (easy-axis) and negative (easy-plane) values of the magnetocrystalline anisotropy coefficient. Analytical work suggests that skyrmion lattice states are minimum energy states only for positive anisotropy values K_1 in the range $[0, 0.48K_0]$,[25] which is in contrast to the wider $[-0.35K_0, 0.55K_0]$ range observed in this work, which includes both positive and negative anisotropy values. There are differences between our work and the model used in Ref. 25 that we believe causes this discrepancy. Firstly, unlike the analytical work, our model includes demagnetization energy, which is known to change skyrmion energetics.[23,39] Secondly, their work identifies skyrmion lattice states as local energy minima and the cone state as the ground state in easy-plane anisotropy systems. In our work, the thinner films suppress conical states,[9] resulting in skyrmion lattice states having the lowest energy. Finally, the chiral twist in the magnetization at the top and bottom of the film, that are known to contribute to the skyrmion stability,[23,45] are accounted for in our model, unlike the two-dimensional analytical model where the skyrmion magnetization does not vary in the thickness direction.

TABLE I. Normalized anisotropy and applied field values for the selected magnetization configurations in Fig. 2 (a) to (f).

	(a)	(b)	(c)	(d)	(e)	(f)
K_1/K_0	0.85	−0.20	−0.35	0.55	0.00	−0.35
$\|\mathbf{H}\|/M_S$	0.0	0.0	0.7	2.1	5.6	9.8

The parameter sets within the solid line in the skyrmion region of Fig. 2 exhibit a hexagonal skyrmion lattice as the minimum energy configuration, as shown in Fig. 2 (e). The magnetization in this simulation cell has a skyrmion number $S \approx 2$. In the remaining skyrmionic region, one skyrmion per simulation cell is found (as in Fig. 2 (d) and (f)), which corresponds to a rectangular skyrmion lattice ($S \approx 1$). The rectangular skyrmion lattice has a lower energy than the hexagonal lattice over most of the parameter space. This occurs because the skyrmion spacing that minimizes the energy changes with the anisotropy, meaning that the hexagonal skyrmions are frustrated in the simulation cell. These two skyrmion lattice configurations compete.[26]

Parameter sets below the solid line in the uniform region of Fig. 2 support local energy minimum (metastable)

skyrmion states, which encompasses most of the parameter space. Fig. 3 shows how metastable skyrmion size changes with anisotropy (snapshots (g), (h) and (i)) and applied field magnitude (snapshots (j), (k) and (l)) at $z = 0$, as parameterized by Table II. Skyrmion size increases with decreasing magnetic field magnitude and increasing easy-plane anisotropy because the magnetization component in the plane is more favorable energetically, which increases the length over which the skyrmion twists. Fig. 3 (i) shows that skyrmions expand to fill the geometry that contains them when easy-plane anisotropy is strong enough. This causes the skyrmion to stretch into two separate objects.[26]

To summarize, skyrmions are minimum energy states in magnetic systems with easy-plane magnetocrystalline anisotropy and demagnetizing effects under micromagnetic simulation. This conclusion is in counterpoint to findings with analytical models,[2,25] but agrees with numerical work that does not consider demagnetization or thickness effects.[26] Systems with weaker easy-plane anisotropy result in smaller skyrmions. Skyrmion lattice states are also metastable in a wide range of anisotropy values. The skyrmion presence as a minimum energy state is consistent with LTEM observations,[36] and supports the interpretation of Hall signals in easy-plane thin films as the topological Hall effect.[28–33] This encourages research into a broader range of materials for skyrmion physics and spintronic applications,[46] as it may enhance the stability of skyrmions in systems where they are already favorable, such as confined geometry materials, and materials with pinning defects.[24]

We acknowledge financial support from EPSRC's DTC grant EP/G03690X/1 and standard research grant EP/J007110/1.

TABLE II. Normalized anisotropy and applied field values for the selected magnetization configurations in Fig. 3 (g) to (l).

	(g)	(h)	(i)	(j)	(k)	(l)
K_1/K_0	0.50	0.00	−0.50	0.00	0.00	0.00
$\lvert\mathbf{H}\rvert/M_S$	10.5	10.5	10.5	15.4	7.0	0.0

[1] T. H. R. Skyrme, Proceedings of the Royal Society of London. Series A. Mathematical and Physical Sciences **260**, 127 (1961).
[2] A. Bogdanov and A. Hubert, J. Magn. Magn. Mater. **138**, 255 (1994).
[3] I. Dzyaloshinsky, J. Phys. Chem. Solids **4**, 241 (1958).
[4] T. Moriya, Phys. Rev. **120**, 91 (1960).
[5] A. Crépieux and C. Lacroix, J. Magn. Magn. Mater. **182**, 341 (1998).
[6] U. Rößler, A. Bogdanov, and C. Pfleiderer, Nat. **442**, 797 (2006).
[7] S. Mühlbauer, B. Binz, F. Jonietz, C. Pfleiderer, A. Rosch, A. Neubauer, R. Georgii, and P. Böni, Science **323**, 915 (2009).
[8] X. Z. Yu, Y. Onose, N. Kanazawa, J. H. Park, J. H. Han, Y. Matsui, N. Nagaosa, and Y. Tokura, Nat. **465**, 901 (2010).
[9] X. Z. Yu, N. Kanazawa, Y. Onose, K. Kimoto, W. Z. Zhang, S. Ishiwata, Y. Matsui, and Y. Tokura, Nat. Mater. **10**, 106 (2011).
[10] S. Seki, X. Yu, S. Ishiwata, and Y. Tokura, Science **336**, 198 (2012).
[11] S. Woo, K. Litzius, B. Krüger, M.-Y. Im, L. Caretta, K. Richter, M. Mann, A. Krone, R. Reeve, M. Weigand, *et al.*, Nat. Mater. (2015).
[12] C. Moreau-Luchaire, C. Moutafis, N. Reyren, J. Sampaio, C. A. F. Vaz, N. V. Horne, K. Bouzehouane, K. Garcia, C. Deranlot, P. Warnicke, P. Wohlhüter, J.-M. George, M. Weigand, J. Raabe, V. Cros, and A. Fert, Nat. Nano., Advance Online Publication (2016).
[13] W. Jiang, P. Upadhyaya, W. Zhang, G. Yu, M. B. Jungfleisch, F. Y. Fradin, J. E. Pearson, Y. Tserkovnyak, K. L. Wang, O. Heinonen, *et al.*, Science **349**, 283 (2015).
[14] O. Boulle, J. Vogel, H. Yang, S. Pizzini, D. d. S. Chaves, A. Locatelli, T. O. M. A. Sala, L. D. Buda-Prejbeanu, O. Klein, M. Belmeguenai, *et al.*, Nat. Nano., Advance Online Publication (2016).
[15] M. E. Stebliy, A. G. Kolesnikov, A. V. Davydenko, A. V. Ognev, A. S. Samardak, and L. A. Chebotkevich, J. Appl. Phys. **117**, 17B529 (2015).
[16] S. Heinze, K. von Bergmann, M. Menzel, J. Brede, A. Kubetzka, R. Wiesendanger, G. Bihlmayer, and S. Blügel, Nat. Phys. **7**, 713 (2011).
[17] S. S. Parkin, M. Hayashi, and L. Thomas, Science **320**, 190 (2008).
[18] F. Jonietz, S. Mühlbauer, C. Pfleiderer, A. Neubauer, W. Münzer, A. Bauer, T. Adams, R. Georgii, P. Böni, R. A. Duine, K. Everschor, M. Garst, and A. Rosch, Science **330**, 1648 (2010).
[19] X. Z. Yu, N. Kanazawa, W. Z. Zhang, T. Nagai, T. Hara, K. Kimoto, Y. Matsui, Y. Onose, and Y. Tokura, Nat. Commun. **3**, 988 (2012).
[20] O. Boulle, G. Malinowski, and M. Kläui, Materials Science & Engineering R **72**, 159 (2011).
[21] A. Fert, V. Cros, and J. Sampaio, Nat. Nano. **8**, 152 (2013).
[22] X. Zhang, M. Ezawa, and Y. Zhou, Sci. Rep. **5**, 9400 (2015).
[23] M. Beg, R. Carey, W. Wang, D. Cortés-Ortuño, M. Vousden, M. Bisotti, M. Albert, D. Chernyshenko, O. Hovorka, R. Stamps, *et al.*, Sci. Rep. **5**, 17137 (2015).
[24] S.-Z. Lin, C. Reichhardt, C. D. Batista, and A. Saxena, Phys. Rev. B **87**, 214419 (2013).
[25] M. N. Wilson, A. B. Butenko, A. N. Bogdanov, and T. L. Monchesky, Phys. Rev. B **89**, 094411 (2014).
[26] S.-Z. Lin, A. Saxena, and C. D. Batista, Phys. Rev. B **91**, 224407 (2015).
[27] J. Rowland, S. Banerjee, and M. Randeria, Phys. Rev. B **93**, 020404 (2016).
[28] S. Huang and C. Chien, Phys. Rev. Lett. **108**, 267201 (2012).
[29] Y. Li, N. Kanazawa, X. Z. Yu, A. Tsukazaki, M. Kawasaki, M. Ichikawa, X. F. Jin, F. Kagawa, and Y. Tokura, Phys. Rev. Lett. **110**, 117202 (2013).
[30] N. A. Porter, P. Sinha, M. B. Ward, A. N. Dobrynin, R. Brydson, T. R. Charlton, C. J. Kinane, M. D. Robertson, S. Langridge, and C. H. Marrows, arXiv preprint arXiv:1312.1722 (2013).
[31] S. A. Meynell, M. N. Wilson, J. C. Loudon, A. Spitzig, F. N. Rybakov, M. B. Johnson, and T. L. Monchesky, Phys. Rev. B **90**, 224419 (2014).
[32] N. A. Porter, J. Carter Gartside, and C. H. Marrows, Phys. Rev. B **90**, 024403 (2014).
[33] T. Yokouchi, N. Kanazawa, A. Tsukazaki, Y. Kozuka, M. Kawasaki, M. Ichikawa, F. Kagawa, and Y. Tokura, Phys. Rev. B **89**, 064416 (2014).
[34] P. Bruno, V. Dugaev, and M. Taillefumier, Phys. Rev. Lett. **93**, 096806 (2004).
[35] B. Binz and A. Vishwanath, Phys. B: Cond. Matt. **403**, 1336 (2008).
[36] X. Yu, A. Kikkawa, D. Morikawa, K. Shibata, Y. Tokunaga, Y. Taguchi, and Y. Tokura, Phys. Rev. B **91**, 054411 (2015).
[37] A. Bogdanov and A. Hubert, J. Magn. Magn. Mater. **195**, 182 (1999).
[38] H. Fangohr, G. Bordignon, M. Franchin, A. Knittel, P. A. de Groot, and T. Fischbacher, J. Appl. Phys. **105**, 07D529

(2009).
[39]F. Rybakov, A. Borisov, and A. Bogdanov, Phys. Rev. B **87**, 094424 (2013).
[40]D. Fredkin and T. Koehler, IEEE Trans. Magn. **26**, 415 (1990).
[41]P. Sinha, N. A. Porter, and C. H. Marrows, Phys. Rev. B **89**, 134426 (2014).
[42]T. Fischbacher, M. Franchin, G. Bordignon, and H. Fangohr, IEEE Trans. Magn. **43**, 2896 (2007).
[43]A. Logg and G. N. Wells, ACM Transactions on Mathematical Software **37** (2010).
[44]P. Bak and M. H. Jensen, Journal of Physics C: Solid State Physics **13**, L881 (1980).
[45]A. Leonov, Y. Togawa, T. Monchesky, A. Bogdanov, J. Kishine, Y. Kousaka, M. Miyagawa, T. Koyama, J. Akimitsu, T. Koyama, *et al.*, arXiv preprint arXiv:1512.04179 (2015).
[46]Y. Tokunaga, X. Z. Yu, J. S. White, H. M. Rønnow, D. Morikawa, Y. Taguchi, and Y. Tokura, Nat. Commun. **6**, 7638 (2015).